

# The Role of Lattice Anion Vacancies in the Activation of CO and as the Catalytic Site for Methanol Synthesis over Zirconium Dioxide and Yttria-Doped Zirconium Dioxide

RONALD G. SILVER,\* CHEINCHANG J. HOU,† AND JOHN G. EKERDT\*

\*Department of Chemical Engineering, †Center for Materials Science and Engineering, The University of Texas at Austin, Austin, Texas 78712

Received January 6, 1989; revised April 13, 1989

The role of lattice oxygen anion vacancy sites in the activation of CO and in the synthesis of methanol was investigated over  $ZrO_2$ . The study involved a comparison of the amounts of CO and  $SO_3$  which adsorbed, the amount of methoxide which could be titrated from zirconia, and the rate of catalytic synthesis of methane and methanol as a function of crystalline phase, calcination conditions, and  $Y_2O_3$  levels in yttria-doped  $ZrO_2$ . Infrared and temperature-programmed desorption results established that CO adsorbed as formate and that  $SO_3$  adsorbed as the sulfate  $(ZrO)_3S=O$ . Uptake studies over yttria-doped  $ZrO_2$  demonstrate that  $SO_3$  interacts with anion vacancy sites to form the sulfate. A maximum in  $SO_3$  and CO adsorption and methanol titration occurred at yttria dopant levels where ionic conductivity is highest for yttria-doped  $ZrO_2$ . The correspondence between the amount of formate or sulfate adsorbed and the amount of methanol produced form the basis for concluding that surface oxygen anion vacancies are the catalytic sites for CO activation and methanol synthesis. © 1989 Academic Press, Inc.

## I. INTRODUCTION

Zirconium dioxide has been shown to be an effective catalyst for the conversion of synthesis gas to branched chain hydrocarbons in a process known as isosynthesis (1-3). Previous results from our laboratory and elsewhere have suggested that the primary products of CO hydrogenation over  $ZrO_2$  at 1 atm are methane and methanol (4-7). Oxygen labeling studies (7) showed that lattice oxygen incorporated into methanol and led to the proposed mechanism in which CO reacted with  $ZrO_2$  to form a formate which was reduced to a methoxide. Methoxide was shown to be the immediate precursor to methane and methanol via hydrogenation and hydrolysis, respectively. Pretreatment of  $ZrO_2$  in  $O_2$  and then  $H_2$  versus only  $O_2$  affected the amount of methanol formed and led to the suggestion that the active site for CO hydrogenation over  $ZrO_2$  was an oxygen anion vacancy (7). The study reported here was undertaken to

measure anion vacancy concentration and to determine if anion vacancies are the active site for CO activation.

Sulfur trioxide was selected as an anion vacancy titrant for  $ZrO_2$  on the basis of studies with  $SO_3$  over other oxides and on the ability to form sulfate species over  $ZrO_2$ . Infrared studies over  $Fe_2O_3$  by Yamaguchi *et al.* (8) showed that sulfur trioxide adsorbed as a sulfate species with a dioxo structure  $(FeO)_2S(=O)_2$ . This was proposed to occur at oxygen anion vacancy sites. A sulfate species could also be formed over  $Fe_2O_3$  from  $SO_2$  in excess  $O_2$  or by calcining  $(NH_4)_2SO_4$  and  $Fe(OH)_3$  (8). A similar sulfate structure with dioxo ligands was proposed by Jin *et al.* (9) following calcination of  $(NH_4)_2SO_4$  and  $Zr(OH)_4$  at 600°C. A recent infrared study by Bensitel *et al.* (10) found that adsorption of  $H_2S$  or  $SO_2$  in excess  $O_2$  over  $ZrO_2$  at 450°C resulted in the  $(ZrO)_3S=O$  sulfate species. This same  $(ZrO)_3S=O$  sulfate structure was also reported following impregnation

of ZrO<sub>2</sub> with H<sub>2</sub>SO<sub>4</sub>, (NH<sub>4</sub>)<sub>2</sub>SO<sub>4</sub>, or Zr(SO<sub>4</sub>)<sub>2</sub> followed by evacuation at 450°C (10).

The oxides of zirconium form three different phases, monoclinic, tetragonal, and cubic (11–13). The monoclinic phase is stable below 1200°C. The tetragonal phase is normally stable above 1200°C, but can be obtained in a metastable condition at much lower temperatures and is the crystal structure of ZrO<sub>2</sub> particles under 300 Å in diameter (14). The cubic phase is formed at temperatures above 2280°C, but can be stabilized at room temperature by the addition of other oxides such as Y<sub>2</sub>O<sub>3</sub> and CaO. Cubic ZrO<sub>2</sub> has a fluorite structure.

Stabilization of the cubic structure is accomplished by direct substitution of di- or trivalent cations of appropriate size for the host lattice Zr<sup>4+</sup> cation. (6 to 8% Y<sub>2</sub>O<sub>3</sub> is required to stabilize the cubic phase (15)). Since the dopant cation is of lower valence than the host cation, oxygen vacancies are created to preserve lattice neutrality. These vacancies increase the electrical conductivity, with diffusing oxygen ions being the primary charge carrier (15–17). This diffusion of oxygen ions has been associated with lattice vacancy migration (15, 16). For the case of yttria-stabilized zirconia (YSZ), spectroscopic studies have shown that the trivalent and tetravalent cations are statistically distributed (18) and that the Zr cations are nearest neighbors to the anion vacancies (19). The electrical conductivity of YSZ reaches a maximum at about 10 mole% Y<sub>2</sub>O<sub>3</sub> and then decreases rapidly (20). The decrease in conductivity with increasing dopant ion concentration has been associated with dopant–vacancy interactions, vacancy–vacancy interactions, or the formation of microdomains (21).

This paper addresses the identity of the site for CO activation over ZrO<sub>2</sub>. Carbon monoxide adsorption was employed to titrate the sites where formate species form and SO<sub>3</sub> adsorption was employed to titrate the anion vacancy sites. Methanol and methane formation were monitored to es-

tablish the amount of methoxide formed. Yttria-doped ZrO<sub>2</sub> was employed as a means to calibrate CO and SO<sub>3</sub> adsorption and methanol titration, since the relative number of anion vacancies could be adjusted by the dopant concentration.

## II. EXPERIMENTAL

All catalysts were prepared from chloride precursors. Zirconia was prepared by dissolving ZrCl<sub>4</sub> in distilled water. Yttria-doped ZrO<sub>2</sub> was prepared by mixing YCl<sub>3</sub> and ZrCl<sub>4</sub> powders prior to dissolving in distilled water. Pure Y<sub>2</sub>O<sub>3</sub> was prepared from YCl<sub>3</sub>. Ammonium hydroxide was added to the salt solutions to form a gel. The gels were washed to a pH of 7 with distilled water until the resulting wash water tested negative for chloride contamination with silver nitrate solution. The gels were then dried in air for 24 h at 120°C, calcined for 2 to 6 h at 600 to 900°C, and quenched in room temperature air immediately after calcining.

Several techniques were used to characterize the catalysts. BET surface area was determined using a Micrometrics 2000 surface analyzer. Phase composition was determined from the X-ray powder diffraction patterns which were obtained on a Phillips diffractometer with a CuK $\alpha$  source. X-ray photoelectron spectroscopy was performed on a VG Scientific Ltd. spectrometer. A JEOL 200CX transmission electron microscope was used with an accelerating voltage of 200 kV for the microscopy studies.

The experimental apparatus and the general techniques for a methanol titration have been presented earlier (7). For the methanol titration studies, approximately 2 g of catalyst were loaded into a 12.70-mm-o.d. quartz tube and were pretreated as follows. The catalyst was heated to 620°C in flowing O<sub>2</sub> and held at this temperature for 10 min. While at 620°C, the tube was flushed with argon for 15 min and finally with H<sub>2</sub> for 10 min. The catalyst was then cooled to 25°C in flowing argon. After pretreatment, water vapor was introduced to

the catalyst by sparging argon through distilled water at 25°C for 8 min. (All gases were at 1 atm and were maintained at a flow rate of 30 ml min<sup>-1</sup>.) A 1/1 mixture of CO/H<sub>2</sub> then flowed over the catalyst for 50 min; during this time the temperature was first ramped to 620°C and then reduced to 25°C. (Heating in CO/H<sub>2</sub> formed methoxide on the surface (7).) The temperature was then increased, under flowing CO/H<sub>2</sub>, to 290°C and water vapor was introduced to the CO/H<sub>2</sub> stream. The reactor effluent composition was determined on a Varian 2400 gas chromatograph equipped with a flame ionization detector and a 1.83 m × 3.2 mm-o.d. column of 50/80 mesh Poropak Q.

The steady-state catalytic formation of methane and methanol was measured using the same apparatus that was used for methanol titration. Sample pretreatment in O<sub>2</sub>, H<sub>2</sub>, and water vapor was also the same. Following exposure to water vapor, the catalyst was heated to 580°C in a 1/1 CO/H<sub>2</sub> mixture (30 ml min<sup>-1</sup>). The temperature was maintained at 580°C for a period of 20 h. The reactor effluent was analyzed by GC. Steady state (defined as constant production of methane and methanol over a two hr period) was usually reached after 17 to 18 h.

The CO temperature-programmed studies followed the procedures of He and Ekerdt (22). The catalyst was pretreated in oxygen at 620°C for 20 min and cooled to 25°C in Ar. The catalyst was subsequently heated in flowing CO while the effluent was monitored with a mass spectrometer.

For the thermogravimetric experiments, approximately 50 mg of catalyst was loaded into the sample pan of a DuPont Instruments 952 thermogravimetric analyzer and pretreated O<sub>2</sub>, Ar, and H<sub>2</sub> at 600°C as described above and cooled to the dose temperature in Ar. The sensitivity of the balance was typically 0.01 mg. The weight of the sample after pretreatment was recorded, and then the catalyst was dosed with the adsorbate gas while monitoring the weight gain with a DuPont Instruments 990

thermal analyzer. Carbon monoxide was dosed at 1 atm and 30 ml min<sup>-1</sup> flow for 30 min while the catalyst was maintained at 500°C. Sulfur trioxide was introduced by sparging Ar through a container of 30% oleum, which was maintained at 0°C. The catalyst was maintained at 110°C and the system pressure was maintained under a partial vacuum of 200 mTorr during the 30-min exposure to SO<sub>3</sub>. The SO<sub>3</sub> adsorption conditions were selected to minimize readorption of water on ZrO<sub>2</sub> during the dosing phase.

The infrared experiments were conducted in a quartz cell equipped with either KBr or CaF<sub>2</sub> optics. Approximately 50 mg of powder was used to press 1 cm diameter, self-supporting disks. The disks were positioned in a high temperature zone in the cell and heated to 620°C in O<sub>2</sub> and maintained at 620°C for 10 min. The cell was evacuated (<5 mTorr) and flushed with argon at 620°C and cooled to 25°C. The cell was evacuated, filled with H<sub>2</sub>, ramped to 620°C, held for 10 min at 620°C, and cooled back to 25°C in H<sub>2</sub>. A reference spectrum of the pretreated disk was recorded, following evacuation at 25°C, using a Digilab FTS 15/90 Fourier transform infrared spectrometer. Carbon monoxide was dosed at 500°C and the resulting spectra were recorded at 25°C. The disk was maintained at 110°C and 200 mTorr during SO<sub>3</sub> dosing, the cell was evacuated to remove the gas phase, and the spectra were recorded at 110°C.

All gases were UHP grade from Big Three Industries. Hydrogen (99.999%) was passed through a deoxo cylinder and a bed of 4A molecular sieves to remove oxygen and water. Carbon monoxide (99.8%) was heated to 180°C over molecular sieves to decompose metal carbonyls. Oxygen (99.9+%) and argon (99.9999%) were passed through a bed of 4A molecular sieves to remove water. Sulfur trioxide was obtained as a 30% oleum from Stauffer Chemical Co. The ZrCl<sub>4</sub> (99.6%) and YCl<sub>3</sub> (99.9%) salts were obtained from Alfa Products.

TABLE 1  
Catalyst Preparation and Composition

Catalyst sample	Calcination temperature (°C)	Calcination time (hr)	BET surface area (m <sup>2</sup> /g)	Composition <sup>a</sup> (Zr/Y)	Phase <sup>b</sup> (M/T/C)
1	600	2 <sup>c</sup>	30.04	100.0/0.0	67/33/0
2	600	4	27.83	100.0/0.0	70/30/0
3	600	6	18.08	100.0/0.0	73/27/0
4	700	4	8.16	100.0/0.0	79/21/0
5	800	4	8.70	100.0/0.0	90/10/0
6	900	5	10.18	100.0/0.0	100/0/0
7	600	4	59.33	96.7/3.3	0/90/10
8	600	4	61.72	95.0/5.0	0/56/44
9	600	4	73.80	93.0/7.0	0/20/80
10	900	5	29.50	93.0/7.0	0/15/85
11	600	4	74.69	90.9/9.1	0/0/100
12	600	4	96.44	90.2/9.8	0/0/100
13	900	5	30.94	90.2/9.8	0/0/100
14	600	4	63.40	88.2/11.8	0/0/100
15	900	5	21.95	88.2/11.8	0/0/100
16	600	4	82.02	85.0/15.0	0/0/100
17	600	4	71.20	80.1/19.9	0/0/100
18	600	4	11.86	0.0/100.0	—

<sup>a</sup> Mole percent ZrO<sub>2</sub> and Y<sub>2</sub>O<sub>3</sub> present.

<sup>b</sup> Percentage of monoclinic, tetragonal, and cubic phases present.

<sup>c</sup> Removed from the oven immediately after calcination and cooled to 25°C.

### III. RESULTS

Tables 1 and 2 summarize the characterization of the catalysts. Table 1 lists the calcination temperatures and times along with the percentage of monoclinic, tetragonal, and cubic ZrO<sub>2</sub> present. Relative amounts of monoclinic, tetragonal, and cubic phases were determined using the method of Evans *et al.* (12). As calcination time and temperature were increased, the BET area decreased to a value near 10 m<sup>2</sup> g<sup>-1</sup> and the percentage of monoclinic ZrO<sub>2</sub> increased to 100 for the pure ZrO<sub>2</sub> samples (catalyst samples 1–6). The phase change is consistent with sintering studies of ZrO<sub>2</sub> powder (14). Yttria levels above 9% resulted in fully stabilized cubic zirconia. Lattice parameters were determined for the cubic zirconias (catalyst samples 11–17) and compared well with the results given by Ingel and Lewis (23).

Table 2 presents a comparison of the bulk

and surface composition for the yttria-doped zirconias. Bulk composition was determined by atomic absorption. The surface composition was determined by comparing the O 1s, Zr 3d, and Y 3d peak areas for the samples against standards consisting of physical mixtures of ZrO<sub>2</sub> and Y<sub>2</sub>O<sub>3</sub>. The

TABLE 2  
Bulk and Surface Composition of Yttria-Doped Zirconias

Catalyst sample	Mole percent Y <sub>2</sub> O <sub>3</sub> in the bulk	Mole percent Y <sub>2</sub> O <sub>3</sub> on the surface
7	3.3	2.7
8	5.0	4.3
9	7.0	6.8
11	9.1	8.5
14	11.8	11.6
16	15.0	13.8
17	19.9	17.2

XPS results have an uncertainty of 1%. The bulk composition corresponded within 0.2 mole% to the composition expected from the chloride salt mixtures. There were slight differences between the bulk and the surface composition.

Figures 1 and 2 present representative transmission electron microscopy results over pure  $\text{ZrO}_2$  and yttria-doped  $\text{ZrO}_2$ , respectively. All the pictures are shown at the same magnification. The effect of calcination temperature and time on the grain morphology of the agglomerated  $\text{ZrO}_2$  particles can be seen in Fig. 1. The average grain size increased with the calcination time at  $600^\circ\text{C}$  and with increasing calcination temperature. The average grain sizes were 10–75, 25–75, 20–90, 25–125, 40–125, and 60–125 nm for calcination at  $600^\circ\text{C}$  and 2, 4, and 6 h, at  $700^\circ\text{C}$  and 4 h, at  $800^\circ\text{C}$  and 4 h, and at  $900^\circ\text{C}$  and 5 h, respectively. The bonding between the particles changed from point contact to surface sharing and the individual particle shape changed from irregular to more or less equiaxed as the calcination time and temperature were increased.

The particle morphology of the yttria-doped  $\text{ZrO}_2$  samples did not show any apparent differences as the yttria content changed. The particle sizes were all about the same for the yttria-doped  $\text{ZrO}_2$  samples calcined at  $600^\circ\text{C}$ , with an average particle diameter of 2–20 nm. Pure  $\text{ZrO}_2$  which was subjected to the same calcination conditions had an average particle diameter of 25–75 nm. In general the  $600^\circ\text{C}$  calcined, yttria-doped  $\text{ZrO}_2$  particles were irregularly shaped and had more point contact than surface sharing between particles. Transmission electron microscopy studies were also conducted with yttria-doped samples calcined at  $900^\circ\text{C}$ . Grain size was seen to increase as expected from the BET measurements. It was not possible to detect changes in particle morphology with increasing calcination temperature.

The IR spectra for  $\text{SO}_3$  adsorbed on  $\text{ZrO}_2$  at  $100^\circ\text{C}$  are characterized by an intense absorbance in the region  $1350\text{--}1400\text{ cm}^{-1}$  and

a complex set of absorbances in the region  $1100\text{--}900\text{ cm}^{-1}$ . Figure 3 presents the changes in the region  $1350\text{--}1400\text{ cm}^{-1}$  with increasing exposure to  $\text{SO}_3$ . (The region  $1100\text{--}900\text{ cm}^{-1}$  is not presented because the bands were poorly resolved. The absorbance intensity in the region  $1100\text{--}900\text{ cm}^{-1}$  increased in parallel with the region  $1350\text{--}1400\text{ cm}^{-1}$ .) The  $\text{SO}_3$  was incrementally dosed by opening a stopcock, for a short time interval, between the IR cell and the  $\text{SO}_3$ /oleum saturator. The amount admitted in each increment cannot be determined. Two bands are seen initially in Spectrum B at  $1357$  and  $1373\text{ cm}^{-1}$ . With increasing exposure the higher frequency band intensity increased more rapidly than the low frequency band and shifted to higher wavenumbers (Spectrum C). The intensity maximum shifted to  $1387$  and finally  $1406\text{ cm}^{-1}$ . A band can also be seen at  $1392\text{ cm}^{-1}$  in Spectrum E. The adsorbed sulfate was removed by heating the  $\text{ZrO}_2$  in  $\text{O}_2$  for 30 min at  $620^\circ\text{C}$  (Spectrum F). In other experiments (not shown) when  $\text{SO}_3$  was dosed for longer periods than for Fig. 3, the spectrum was similar to that shown in Fig. 3E with the maximum centered between  $1400$  and  $1406\text{ cm}^{-1}$ . This saturation spectrum (Fig. 3E) could be removed by heating the IR disk in  $\text{O}_2$  at  $620^\circ\text{C}$  for 30 min and then reformed by subsequent exposure to  $\text{SO}_3$ .

Infrared experiments of  $\text{SO}_3$  adsorption on yttria-doped  $\text{ZrO}_2$  could not be performed because intense Y–O–Zr lattice stretches between  $1700$  and  $1250\text{ cm}^{-1}$  obscured the region of interest.

Gravimetric experiments were performed to determine if  $\text{SO}_3$  was reacting with adsorbed oxygen or hydroxyl groups, which could form during pretreatment. Following the standard  $\text{O}_2/\text{H}_2$  pretreatment and initial  $\text{SO}_3$  uptake for 30 min the sample was subjected to desorption in  $\text{O}_2$ ,  $\text{O}_2$  and then  $\text{H}_2$ , or Ar for 15 min at  $600^\circ\text{C}$ , cooled to  $110^\circ\text{C}$ , and then reexposed to  $\text{SO}_3$ . This process of desorption/adsorption was repeated many times and the results are presented in Fig. 4. Figure 4B shows the sam-

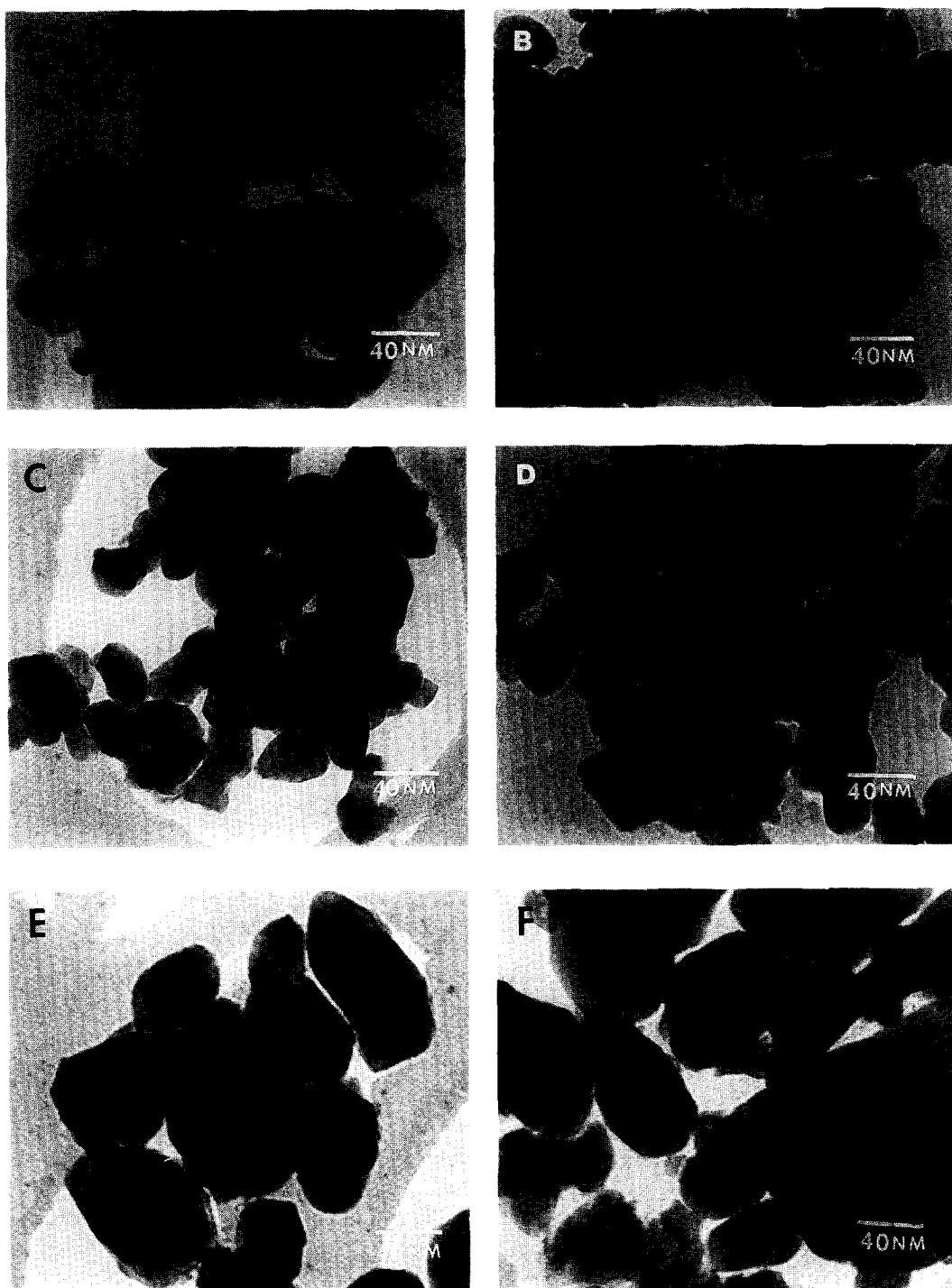


FIG. 1. Transmission electron microscopy results for pure  $\text{ZrO}_2$  subjected to different calcination conditions: (A)  $600^\circ\text{C}$  for 2 h, (B)  $600^\circ\text{C}$  for 4 h, (C)  $600^\circ\text{C}$  for 6 h, (D)  $700^\circ\text{C}$  for 4 h, (E)  $800^\circ\text{C}$  for 4 h, and (F)  $900^\circ\text{C}$  for 5 h.

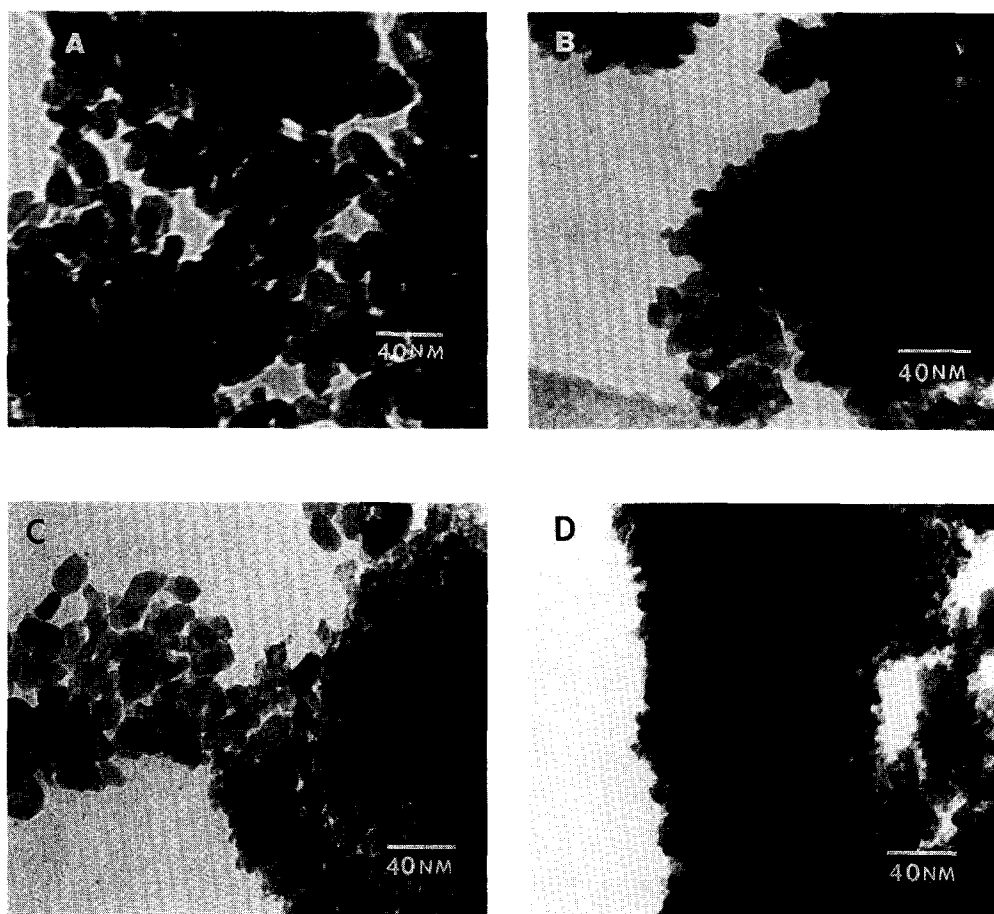


FIG. 2. Transmission electron microscopy results for yttria-doped  $ZrO_2$  calcined at  $600^\circ C$  for 4 h with different mole percent  $Y_2O_3$ : (A) 3.3, (B) 9.1, (C) 11.8, and (D) 15.0

ple weight following repeated doses of  $SO_3$  and desorption in argon. The net weight gain for each adsorption is presented in curve 3 of Fig. 4A for the data presented in Fig. 4B. The weight of  $SO_3$  adsorbed is also shown in Fig. 4A for the different desorption conditions over  $ZrO_2$  (catalyst sample 2) and for 9.1%  $Y_2O_3$  (catalyst sample 11). The weight gain eventually reached a constant value with increasing dose number, for each desorption condition, suggesting that  $SO_3$  was not reacting with species formed during desorption and that  $SO_3$  was reversibly adsorbed.

Weight change was also monitored for catalyst sample 2 which was subjected to the standard pretreatment and held in 200

mTorr of Ar in place of a 200-mTorr mixture of  $SO_3/Ar$ . Following the 30-min 200-mTorr exposure the catalyst was heated to  $600^\circ C$  in Ar (at 1 atm) and cooled back to  $110^\circ C$ , and the cycle was repeated. The weight did not change during five cycles indicating that weight changes observed in Fig. 4 are associated with removal and readsorption of  $SO_3$ . Our ability to adsorb  $SO_3$  reversibly, seen both in Fig. 4 and in the IR experiments described above, implies that multilayers of sulfate did not form.

The typical  $SO_3$  adsorption experiment involved pretreatment in  $O_2/H_2$  and dosing at  $110^\circ C$  for 30 min. The weight change during exposure to  $SO_3$  was observed to in-

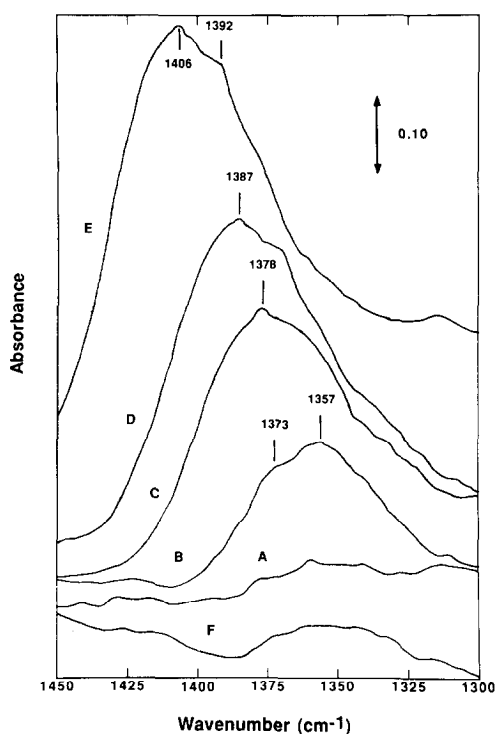


FIG. 3. Spectra recorded following exposure of catalyst sample 2 to SO<sub>3</sub> at 110°C and 200 mTorr for different amounts of time. The cell was evacuated (5 mTorr) prior to collecting each spectrum. Spectrum A is the background. Spectra B–E are for sequential dosing of the same sample after 6.0 min (B), 6.66 min (C), 7.0 min (D), and 7.66 min (E). Spectrum F was recorded after E and heating the catalyst to 620°C in O<sub>2</sub> for 30 min.

crease rapidly within the first 10 min and remained relatively constant for 15 min, after which it would begin to increase again. This second increase could have resulted from oligomers of S<sub>x</sub>O<sub>y</sub>, such as the S<sub>2</sub>O<sub>7</sub> species suggested by Bensitel *et al.* (10) at high doses of SO<sub>2</sub>. The SO<sub>3</sub> uptake results are reported in Table 3 and refer to the amount adsorbed after 20 min.

Previous IR studies with ZrO<sub>2</sub> have demonstrated that CO adsorbs as a formate (24). Formate formation was confirmed over ZrO<sub>2</sub> catalyst samples 1–5 using IR. Adsorption of CO at 500°C produced only the characteristic absorbance bands at 2875, 1387, 1580, and 1360 cm<sup>-1</sup> corre-

sponding to the  $\nu$  C–H,  $\delta$  C–H,  $\nu$  COO<sup>-</sup>(as), and  $\nu$  COO<sup>-</sup>(sy) modes, respectively. An absorbance band was observed at 2915 cm<sup>-1</sup> over yttria-doped ZrO<sub>2</sub> following CO adsorption at 500°C. Formate  $\delta$  C–H,  $\nu$  COO<sup>-</sup>(as), and  $\nu$  COO<sup>-</sup>(sy) bands could not be observed over yttria-doped ZrO<sub>2</sub> samples because the region from 1700 to 1250 cm<sup>-1</sup> was obscured by oxide lattice absorbance bands.

A series of temperature-programmed desorption (TPD) studies was performed to test for the formation of formate over the yttria-doped ZrO<sub>2</sub> samples which were calcined at 600°C and two of the ZrO<sub>2</sub> samples (catalyst samples 4 and 6). Previous TPD studies over ZrO<sub>2</sub> had shown that pretreatment in O<sub>2</sub> followed by programmed heating in CO resulted in the simultaneous formation of CO<sub>2</sub>, CH<sub>4</sub>, and H<sub>2</sub> at 580–620°C, which was associated with formate formation from CO and its subsequent decomposition (22). The TPD studies over the ZrO<sub>2</sub> samples reproduced the results reported in Fig. 3 of Ref. (22); a small desorption peak for bicarbonate was seen along with the large formate desorption peak. The yttria-doped ZrO<sub>2</sub> samples produced the characteristic pattern for formate at 580–620°C and showed no evidence that bicarbonate had formed.

Programmed heating of pure Y<sub>2</sub>O<sub>3</sub> (catalyst sample 18) in CO revealed the evolution of CO<sub>2</sub> and H<sub>2</sub>, but no CH<sub>4</sub>, at the formate desorption temperature (580–620°C). No evidence for bicarbonate was seen. The appearance of CH<sub>4</sub> over ZrO<sub>2</sub> has been used to argue for the presence of a formate on the surface (22). Formate may have been present over Y<sub>2</sub>O<sub>3</sub> but decomposed to give different products than are seen over ZrO<sub>2</sub>.

The gas phase was monitored during exposure of ZrO<sub>2</sub>, yttria-doped ZrO<sub>2</sub> samples 8 and 17, and pure Y<sub>2</sub>O<sub>3</sub> to CO at 500°C. The samples were pretreated in O<sub>2</sub> and H<sub>2</sub> at 620°C and cooled to 500°C in flowing Ar. The effluent composition was continuously monitored as the flowing gas was switched from Ar to CO. There was no evidence that

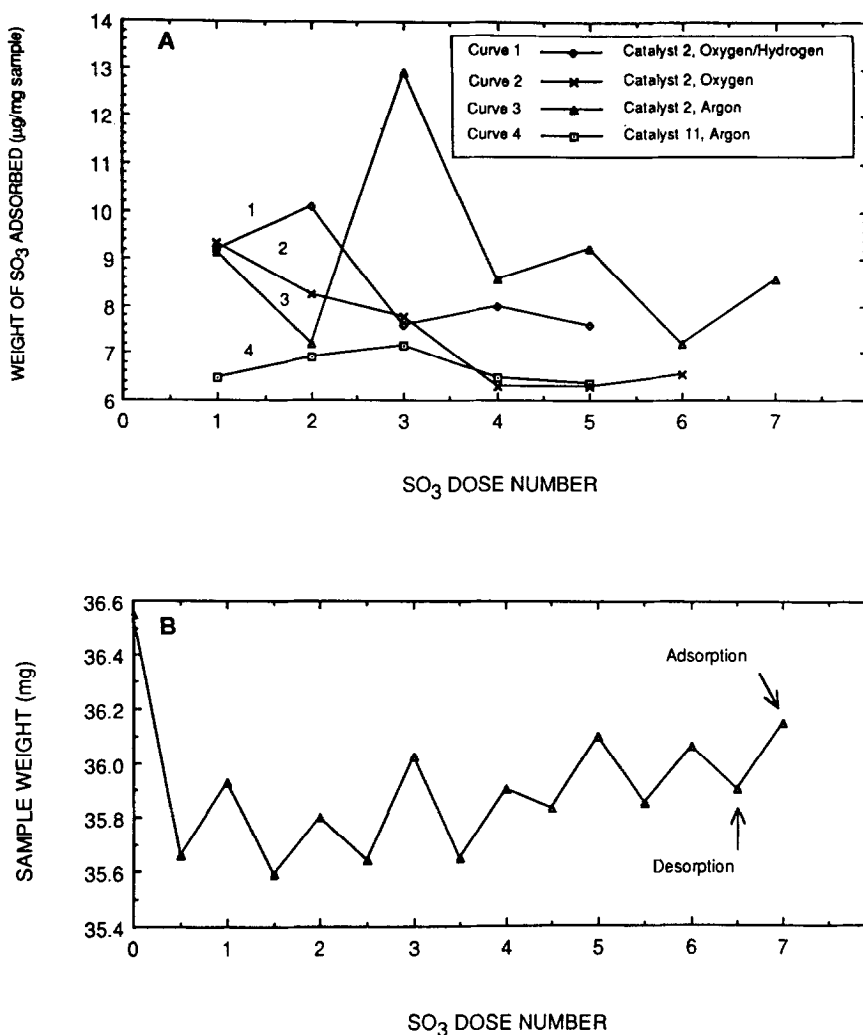


FIG. 4. (A) Weight of SO<sub>3</sub> adsorbed versus dose number for catalyst sample 2 following desorption between doses in O<sub>2</sub> and then H<sub>2</sub> (curve 1), O<sub>2</sub> (curve 2), and argon (curve 3), and for catalyst sample 11 following desorption in argon (curve 4). (B) Sample weight during the course of the repeated dose experiment for catalyst sample 2 subjected to desorption in argon. SO<sub>3</sub> dose numbers 0.0 and 0.5 designate the initial sample weight and following pretreatment, respectively. Integer dose numbers refer to the sample weight following adsorption.

CO<sub>2</sub> formed and desorbed during exposure to CO at 500°C. Previous studies (25) have shown that CO<sub>2</sub> leads to the formation of bicarbonate and carbonates over ZrO<sub>2</sub>.

The IR and TPD studies were undertaken to determine if species other than formate formed during the CO uptake experiments at 500°C. The results support the formation of formate on both ZrO<sub>2</sub> and yttria-doped ZrO<sub>2</sub> and do not indicate that other species

were present. The CO uptake results are listed in Table 3.

The methanol titration results are also listed in Table 3. Methoxide was formed during cooling from 600 to 290°C in CO/H<sub>2</sub>. This methoxide was hydrolyzed by water added at 290°C. The precedence for this process has appeared in the literature (7). The effluent composition of methanol decreased with time after exposure of the cat-

TABLE 3  
Gravimetric Uptake, Titration, and Synthesis Results

Catalyst sample	Molecules SO <sub>3</sub> adsorbed/m <sup>2</sup> ( $\times 10^{-17}$ )	Molecules CO adsorbed/m <sup>2</sup> ( $\times 10^{-17}$ )	Molecules CH <sub>3</sub> OH titrated/m <sup>2</sup> ( $\times 10^{-17}$ )	C <sub>1</sub> rate molecules/m <sup>2</sup> sec ( $\times 10^{-12}$ )	Percent CH <sub>3</sub> OH in C <sub>1</sub> products
1	17.1	3.09	7.04	22.5	30.4
2	28.5	6.00	6.61	17.1	33.4
3	43.5	11.1	7.68	27.7	28.7
4	20.5	16.2	14.1	79.7	27.3
5	35.2	18.2	10.9	92.5	29.0
6	40.6	19.2	8.23	32.6	30.1
7	1.57	1.10	0.89	3.50	34.4
8	3.13	1.52	1.15	4.22	37.1
9	4.98	1.88	2.08	4.75	51.5
10	11.5	4.68	4.18	9.54	48.9
11	11.9	3.06	2.64	7.43	52.2
12	9.73	3.23	2.86	7.02	49.6
13	25.9	8.83	6.27	21.9	45.3
14	6.25	1.02	2.14	5.55	48.0
15	15.7	5.11	5.34	13.2	40.7
16	3.94	0.94	0.28	2.82	37.4
17	6.74	1.50	0.20	5.17	26.6
18	8.73	6.02	0.008	14.4	1.1

alyst to CO/H<sub>2</sub>/H<sub>2</sub>O. The composition decay for each catalyst could be fit with a first-order equation; a different time constant was found for each experiment. The amount of methanol reported in Table 3 refers to the area under the first-order decay curves between the time where methanol was first observed and 200 min. In most cases methanol was not detected after 120–130 min; however, when methanol was found in the effluent after 200 min this amount was no greater than 5% of the initial value. Production past 200 min was observed for catalyst sample 7.

The relative spread over each catalyst sample was averaged for each probe molecule as a means of establishing the precision of the data reported in Table 3. The averages of the relative spreads for SO<sub>3</sub>, CO, and methanol titration were 12, 10, and 16%, respectively.

Methanol and methane were formed in a catalytic reaction at 580°C. The C<sub>1</sub> rates listed in Table 3 refer to rates measured after 17 to 18 h. The percentage of methanol

in the catalytic reaction was approximately 30 for ZrO<sub>2</sub>, varied with the yttria loading, and was 1.1 for Y<sub>2</sub>O<sub>3</sub>.

#### IV. DISCUSSION

The interaction of CO and CO/H<sub>2</sub> mixtures with ZrO<sub>2</sub> has been studied, and the species which formed and how they transformed are understood (6, 7, 22, 24). This study was directed at establishing the role of the oxide surface in the activation of CO and in the formation of the C<sub>1</sub> fragments which are involved in methane and methanol formation at 1 atm (7) and in isosynthesis at 35 atm (3). The active site for formate formation and reduction to methoxide had been suggested to be a surface anion vacancy (7). Molecular probes were selected as the means to identify the site over ZrO<sub>2</sub>. Carbon monoxide was expected to form a formate, CO/H<sub>2</sub> adsorption followed by hydrolysis of methoxide to methanol was expected to identify the methoxide surface concentration, and SO<sub>3</sub> was expected to react with anion vacancies and form a sulfate.

Steady-state  $C_1$  synthesis was selected as an independent measure of methoxide formation and to demonstrate the catalytic activity of the different catalysts.

The discussion below is based on parallel trends in uptake as  $ZrO_2$  was altered through thermal treatment or dopant level. For the uptake studies over pure  $ZrO_2$  the calcination temperature and calcination time were varied to determine if the amounts of formate, sulfate, and  $CH_3OH$  could be altered. With higher temperatures and longer calcination times it was thought that defects in the  $ZrO_2$  could be annealed out and the amount of each probe interacting with the surface would decrease. However, sintering of the  $ZrO_2$  occurred and the metastable tetragonal phase transformed into the thermodynamically stable monoclinic phase (14). Calcination conditions did alter the amount of CO and  $SO_3$  adsorbing as formate and sulfate, respectively, and the amount of methoxide formed. The data in Table 3 do show that methanol formation occurred over all three phases of  $ZrO_2$ . The uptake studies were also performed over yttria-doped  $ZrO_2$ . Yttria doping of  $ZrO_2$  was used to generate a single phase (cubic)

in more than one sample and to introduce anion vacancies. The trends in uptake and  $C_1$  synthesis are shown in Fig. 5 for yttria-doped  $ZrO_2$  which was calcined at  $600^\circ C$ .

Infrared studies over  $ZrO_2$  revealed that only formate formed following exposure to CO at  $500^\circ C$ ; carbonates, bicarbonate, or adsorbed CO was not seen. An absorbance band was seen over yttria-doped  $ZrO_2$  at  $2915\text{ cm}^{-1}$  following CO adsorption at  $500^\circ C$ . This  $2915\text{-cm}^{-1}$  band is proposed to be associated with the  $\nu\text{ C-H}$  stretch of a formate because the TPD studies over  $ZrO_2$  and yttria-doped  $ZrO_2$  produced identical formate decomposition patterns ( $CO_2$ ,  $H_2$ , and  $CH_4$  appeared simultaneously) at  $580\text{--}620^\circ C$ . Carbon dioxide was not observed in the gas phase upon exposure of  $ZrO_2$  or yttria-doped  $ZrO_2$  to CO at  $500^\circ C$ , providing evidence that bicarbonate or carbonate species did not form at  $500^\circ C$ . Taken together, the IR and TPD studies provide evidence that weight changes recorded during CO adsorption are associated with the formation of a formate species.

Desorption peaks for  $CO_2$  and  $H_2$  appeared in the TPD experiments over pure  $Y_2O_3$  at the same temperature where for-

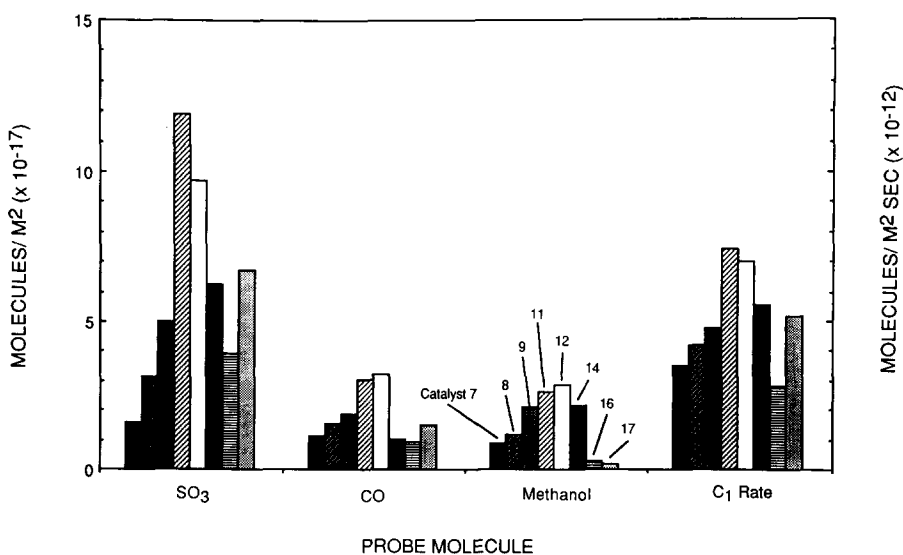


FIG. 5. Amount of  $SO_3$  and CO adsorbed and methanol titrated, and the  $C_1$  synthesis rate per square meter over the yttria-doped  $ZrO_2$  catalysts.

mate decomposition occurs over ZrO<sub>2</sub>. Formate may have been present over Y<sub>2</sub>O<sub>3</sub> because hydrogen desorbed in parallel with CO<sub>2</sub>. Methanol formation was severely inhibited over pure yttria during the titration experiment suggesting that formate reacts differently over Y<sub>2</sub>O<sub>3</sub> than over ZrO<sub>2</sub>. Different reactivity may explain why CH<sub>4</sub> was not observed during the TPD experiment over pure Y<sub>2</sub>O<sub>3</sub>. The other possible source of H<sub>2</sub> along with CO<sub>2</sub> could be a bicarbonate species. However, CO<sub>2</sub> was not formed during CO exposure and bicarbonate formation seems unlikely at 500°C for this reason. Methane was seen in the TPD of CO over the yttria-doped zirconias and the amount of CO adsorbed on yttria-doped ZrO<sub>2</sub> did not increase with increasing yttria loadings (Fig. 5). Regardless of the interaction of CO with pure Y<sub>2</sub>O<sub>3</sub>, the data suggest that CO interacted with ZrO<sub>2</sub> modified by yttria rather than exclusively with surface yttrium cations.

The methanol titration data were identical in form to an earlier study (7). Titration involves first forming methoxide by heating and cooling the catalyst in flowing CO/H<sub>2</sub> and then hydrolyzing the methoxide by exposure of the catalyst to CO/H<sub>2</sub>/H<sub>2</sub>O at 290°C. The hydrolysis reaction was fit with a first-order curve suggesting that no additional methoxide formed during the titration process. Previous studies over ZrO<sub>2</sub> (7) suggest that other species such as carbonates and bicarbonate could be present on the surface as a result of heating the catalyst to 620°C and cooling it back to 25°C in CO/H<sub>2</sub>. Therefore, methanol yields should not be expected to count all of the sites where methoxide can form. Some of the methoxide or methanol may also have been oxidized to other products during hydrolysis and would not have been accounted for in the titration. All of the experiments were performed under identical conditions, possible oxidation losses and less than 100% formation of methoxide at all available sites should have a similar effect on the methanol yields over each catalyst. We propose

that the amount of methanol listed in Table 3 provides a relative measure of the amount of methoxide present when the catalyst was exposed to CO/H<sub>2</sub>/H<sub>2</sub>O. Furthermore, for samples calcined at 600°C, methanol formation displayed a continuous decrease with increasing Y<sub>2</sub>O<sub>3</sub> (above 9.8%) and was barely detected over pure Y<sub>2</sub>O<sub>3</sub> suggesting that methanol is formed over the ZrO<sub>2</sub> sites in yttria-doped ZrO<sub>2</sub>.

There are two issues associated with SO<sub>3</sub>: the structure of the adsorbed species and whether SO<sub>3</sub> reacts with anion vacancy sites during adsorption. The IR studies can be used to assign the structure. The effects of yttria loading are used to address the role of anion vacancy sites.

The infrared spectra for SO<sub>3</sub> adsorption at 110°C are similar to those reported by Bensitel *et al.* (10), who studied the adsorption of SO<sub>2</sub> in an excess of O<sub>2</sub> at 450°C. They reported two bands at 1352 and 1365 cm<sup>-1</sup> following addition of 10 μmol g<sup>-1</sup> of SO<sub>2</sub>. With increasing exposure to SO<sub>2</sub> the 1365-cm<sup>-1</sup> band increased in intensity more rapidly than the 1352-cm<sup>-1</sup> band and its peak maximum shifted to higher wavenumbers (1392 cm<sup>-1</sup> for 250 μmol g<sup>-1</sup> of SO<sub>2</sub>). Beyond 300 μmol g<sup>-1</sup> a peak at 1403 cm<sup>-1</sup> appeared. They also reported six peaks in the region 1200 to 800 cm<sup>-1</sup> which increased in intensity with increasing SO<sub>2</sub> exposure. Bensitel *et al.* proposed that the 1352-cm<sup>-1</sup> and 1365- to 1392-cm<sup>-1</sup> absorbance bands were due to sulfate species with single S=O oscillators, (ZrO)<sub>3</sub>S=O, which were possibly bonded to the different crystal surface faces of ZrO<sub>2</sub>. They ruled out the possibility that Zr-O-SO<sub>2</sub>-O-Zr was formed on the basis of partial <sup>18</sup>O exchange experiments with the sulfate. Only one new band was observed, approximately 40 cm<sup>-1</sup> lower, following partial oxygen exchange. Partially exchanged sulfate with two S=O ligands would have produced three bands whereas partially exchanged sulfate with one S=O ligand would produce only two bands (10). The bands in the region 1200 to 800 cm<sup>-1</sup> were assigned to Zr-O-S stretch-

ing modes on the basis of  $^{18}\text{O}$  labeling studies. Finally, the band which formed at the highest exposures,  $1403\text{ cm}^{-1}$ , was assigned to a  $\text{S}_2\text{O}_7$  species, in which each S has a single  $\text{S}=\text{O}$  ligand and two  $\text{S}-\text{O}-\text{Zr}$  bonds and is bridged with the remaining oxygen ligand.

The amount of  $\text{SO}_3$  dosed into the IR cell cannot be determined, preventing a direct quantitative comparison between changes seen in Fig. 3 with coverage and those reported by Bensitel *et al.* The spectra in both studies are characterized by an intense absorbance in the region  $1400\text{--}1350\text{ cm}^{-1}$  and a complex set of absorbances between  $1150$  and  $900\text{ cm}^{-1}$ . The absorbance maximum at  $1373\text{ cm}^{-1}$  is seen in Fig. 3 to shift to higher wavenumbers, eventually reaching  $1392\text{ cm}^{-1}$ , and increase in intensity with increasing exposure to  $\text{SO}_3$ . An absorbance band can also be seen at  $1357\text{ cm}^{-1}$ . Prolonged exposure to  $\text{SO}_3$  resulted in a band centered between  $1400$  and  $1406\text{ cm}^{-1}$ .

We propose that the  $(\text{ZrO})_3\text{S}=\text{O}$  sulfate species formed over  $\text{ZrO}_2$  from  $\text{SO}_3$  because the absorbance patterns were similar to those reported by Bensitel *et al.* (10). The sulfate structure with dioxo ligands suggested by Jin *et al.* (9), following sulfation of  $\text{ZrO}_2$ , was not considered for the reasons presented by Bensitel *et al.* During the gravimetric  $\text{SO}_3$  studies the weight gain remained constant and then began to increase after about 30 min of  $\text{SO}_3$  exposure. The initial weight gain (reported in Table 3) is proposed to be associated with sulfate formation and the second weight gain we observed is probably associated with oligomers of  $\text{SO}_3$  such as  $\text{S}_2\text{O}_7$ .

The data in Table 3 reveal that  $\text{SO}_3$  adsorbed on pure  $\text{Y}_2\text{O}_3$  (sample 18). Sulfur trioxide is known to form sulfates over other oxides, such as  $\text{Fe}_2\text{O}_3$  (8) and  $\text{SiO}_2$  (26); therefore,  $\text{SO}_3$  interaction with  $\text{Y}_2\text{O}_3$  and the likely formation of a sulfate should be expected. The pattern of uptake with increasing yttria levels (Fig. 5) suggests that  $\text{SO}_3$  did not exclusively interact with surface yttrium cations because uptake should

have, at the very least, increased with dopant level.

All of the probe molecules are seen in Fig. 5 to have a maximum for the 9.1 or 9.8% yttria-doped  $\text{ZrO}_2$  catalyst (catalyst samples 11 and 12). Pure  $\text{Y}_2\text{O}_3$  had a higher uptake of  $\text{SO}_3$  and CO than the 11.8, 15.0, and 19.9% catalysts (Table 3, catalyst samples 14, 16, and 17, respectively). A high surface yttrium cation concentration may explain why the uptake of  $\text{SO}_3$  and CO increased for catalyst 17, which had the highest yttria loading, 19.9%, compared to catalyst 16 (15%  $\text{Y}_2\text{O}_3$ ). The XPS results in Table 2 demonstrate that, within experimental error, there was no surface segregation or depletion of yttria; therefore, the maximum uptake over catalysts 11 or 12 was not associated with an anomalously high surface  $\text{Y}_2\text{O}_3$  concentration. We propose that the maximum uptake over the 9.1 or 9.8% sample is associated with the mobility of anion vacancies. These vacancies are most mobile in the 9.1 or 9.8% catalyst (see below) and are possibly drawn to the surface because the vacancy can undergo reaction with the probe molecules. We also propose that a correlation between anion vacancy mobility and  $\text{SO}_3$  uptake supports the hypothesis that  $\text{SO}_3$  interacts with anion vacancies.

Yttria-stabilized  $\text{ZrO}_2$  belongs to the doped fluorite oxide class of compounds. This class includes Zr, Hf, and Ce oxides doped with Ca, Mg, Y, Yb, Gd, Nd, and other cations. An extensive literature exists for this class of compounds, which discusses the structure and conductivity as a function of dopant type, size, and concentration (13, 15–21, 23, 27–34). The conductivity is ionic and proceeds by vacancy migration. In general, for stabilized  $\text{ZrO}_2$ , the conductivity has a maximum somewhat above the lowest doping level that is required to make the cubic structure (15). Six to eight mole percent yttria is required to stabilize  $\text{ZrO}_2$  fully and the conductivity maximum appears around 10% (20, 21). This could explain why 9.1 or 9.8%  $\text{Y}_2\text{O}_3$

had the greatest interaction with the probe molecules. The conductivity at 15% Y<sub>2</sub>O<sub>3</sub> is an order of magnitude less than the maximum value. The possible causes for this decrease were presented in the Introduction. Decreasing conductivity means that vacancy migration is reduced and vacancies would be less able to migrate to the surface and undergo the reactions proposed above.

Methanol was produced in a noncatalytic reaction during the titration studies to get a relative measure of the number of methoxide species formed as the catalyst was modified by temperature or yttria. Methanol was also produced in a catalytic reaction over ZrO<sub>2</sub> and yttria-doped ZrO<sub>2</sub> at atmospheric pressure. Methoxide is the precursor to methanol in the titration experiments and is the precursor to methane and methanol in the steady-state catalytic reaction (7). The C<sub>1</sub> rate data are presented to show that all the samples were catalysts for CO hydrogenation. With the exception of catalyst samples 4 and 17 the C<sub>1</sub> rate increased as the amount of titrated methanol increased. (A high surface yttrium concentra-

tion may explain why catalyst 17 deviated from the trend.) Correspondence between the rate of methoxide reaction and the amount of methoxide removed during titration supports our use of the titration measurements to obtain a measure of the sites at which methoxide forms.

The SO<sub>3</sub> uptake data and methanol titration data (Table 3) for catalyst samples 1-17 are plotted in Fig. 6. With the exception of the datum point corresponding to catalyst sample 4, which was reproduced several times for SO<sub>3</sub> and methanol, there is a reasonable correlation between the amount of methanol formed and the amount of SO<sub>3</sub> adsorbed as sulfate. Similar correlations (not shown) were found when the amount of CO adsorbed as formate was plotted versus the amount of SO<sub>3</sub> adsorbed or when CO adsorbed was plotted versus methanol formed. Each of these probes involve different surface process: SO<sub>3</sub> adsorbs, CO adsorbs and reacts with a surface OH or H (7), and CO/H<sub>2</sub> adsorb and transform from the formate to the methoxide which is then hydrolyzed and in the presence of CO/H<sub>2</sub>/

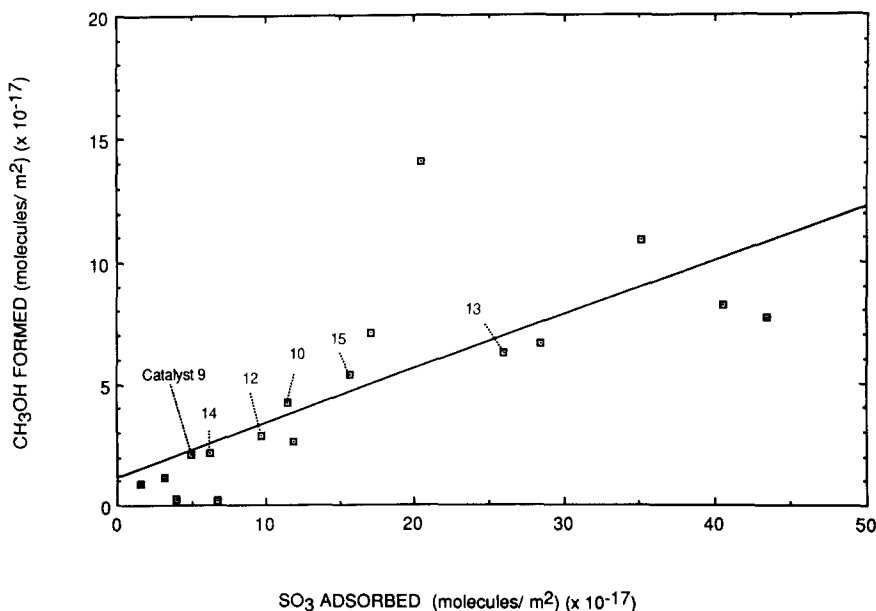


FIG. 6. Molecules of methanol formed per square meter versus the molecules of SO<sub>3</sub> adsorbed per square meter.

H<sub>2</sub>O to methanol, and each was selected to interact differently with the proposed active site. No one physical or chemical property of ZrO<sub>2</sub> could be systematically changed without simultaneously changing other properties. Correlations showing increasing methanol formation or CO adsorption with increasing SO<sub>3</sub> uptake support the proposal made earlier (7) that CO hydrogenation to methanol proceeds over anion vacancy sites.

Catalyst samples which contained different amounts of monoclinic, tetragonal, and cubic ZrO<sub>2</sub> are represented in Fig. 6. The pure ZrO<sub>2</sub> samples displayed a higher uptake of SO<sub>3</sub> and higher amounts of methanol than the yttria-doped ZrO<sub>2</sub> samples. Since yttria introduces anion vacancies one might expect the yttria-doped ZrO<sub>2</sub> samples to display higher uptake. One possible reason the pure ZrO<sub>2</sub> samples had more uptake per unit BET area could be associated with the degree of sintering and grain morphology. The ZrO<sub>2</sub> samples which were subjected to more extreme calcination conditions had well-developed polygonal, equiaxed grains and, in general, a higher uptake than catalyst samples 1 and 2, which had less-developed grains. A more complete discussion of the pure ZrO<sub>2</sub> data is not possible because the ZrO<sub>2</sub> underwent phase change along with sintering. The pictures in Figs. 1 and 2 show that the yttria-doped ZrO<sub>2</sub> samples had grains similar to those for the least-sintered ZrO<sub>2</sub> samples (catalyst samples 1 and 2).

Additional evidence that sintering influences the active site density is found by comparing two sets of yttria-doped ZrO<sub>2</sub> samples which differ by the extent of calcination, catalyst samples 9, 12, and 14, and catalyst samples 10, 13, and 15. The maximum in uptake for the two sets (Table 3) was realized over the 9.8% Y<sub>2</sub>O<sub>3</sub> catalyst for each probe. A maximum at 9.8% Y<sub>2</sub>O<sub>3</sub> reinforces the vacancy migration argument made earlier. The absolute amount of adsorption and C<sub>1</sub> synthesis was found to increase with sintering. (The catalyst samples

in the two sets are indicated in Fig. 6.) The reasons for an increase in uptake with sintering were not revealed by the data. The surface structure of unsupported oxides have been shown to influence the activity and selectivity of oxidation reactions (35–37). Surface structure changes with sintering may have caused the increase in uptake over the yttria-doped ZrO<sub>2</sub> samples.

Figure 7 presents the mechanism for CO interaction with ZrO<sub>2</sub>, which was presented in an earlier publication (7), and a representation of SO<sub>3</sub> reacting with a vacancy site on the ZrO<sub>2</sub> surface. (The (111) face of cubic ZrO<sub>2</sub> was chosen to simplify the figure.) Hydroxyl groups are not shown in Fig. 7A because our studies did not indicate any role of hydroxyl groups in sulfate formation. (Hydroxyl groups were present during all of the experiments.) Desorption in argon or oxygen, during the repeated dose experiments (Fig. 4), should have prevented repopulation of hydroxyl groups. If hydroxyl groups play a role in the uptake of SO<sub>3</sub>, this would have led to a continuous decrease in SO<sub>3</sub> uptake with continued dosing/desorption cycles. Bensitel *et al.* (10) also did not find any infrared evidence for hydroxyl interaction with SO<sub>2</sub> during sulfate formation.

## V. SUMMARY

Sulfur trioxide, CO, and CO/H<sub>2</sub> were used in adsorption and titration experiments to determine if surface oxygen anion vacancies are the active site for CO hydrogenation over ZrO<sub>2</sub>. Infrared spectroscopy and TPD were used to establish that CO adsorbed as a formate and IR was used to establish that SO<sub>3</sub> adsorbed as the (ZrO)<sub>3</sub>S=O sulfate. Yttria-doped ZrO<sub>2</sub> was employed as a means to investigate if SO<sub>3</sub> adsorbed at the anion vacancy sites because the relative vacancy level could be adjusted by changing the amount of Y<sub>2</sub>O<sub>3</sub>. A correlation between the amount of SO<sub>3</sub> adsorbed and the vacancy mobility in yttria-doped ZrO<sub>2</sub> formed the basis for proposing that SO<sub>3</sub> titrates the anion vacancy sites on the surface of ZrO<sub>2</sub>. The SO<sub>3</sub> mole-

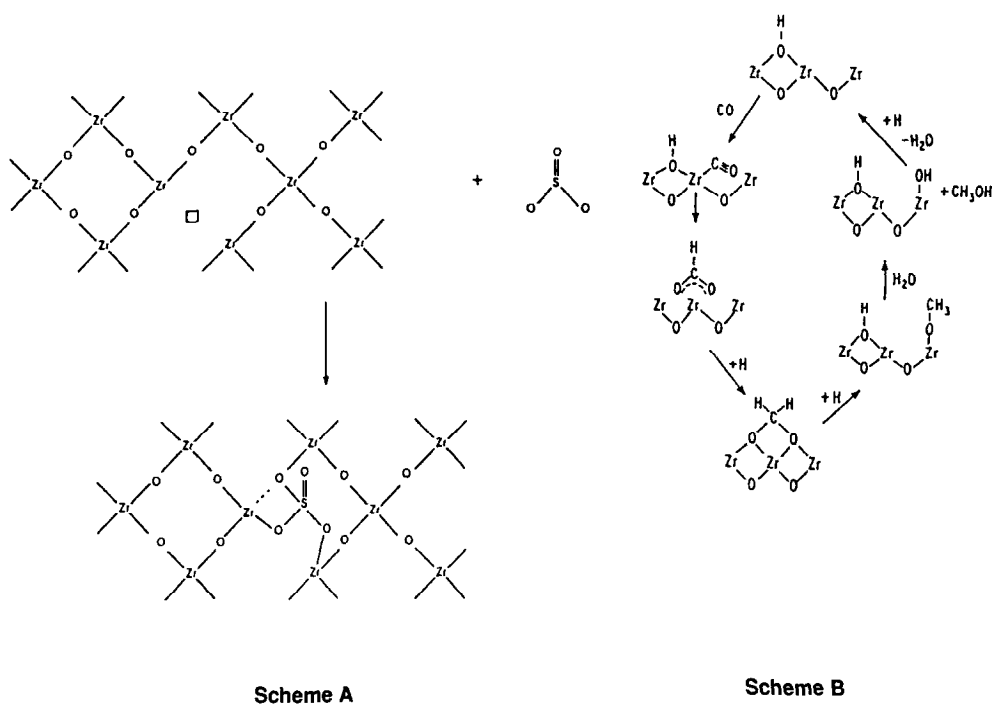


FIG. 7. Proposed scheme for the interaction of the probe molecules with  $ZrO_2$ . (Scheme B was taken from Ref. (7).)

cules react with anions at the vacancy in addition to occupying the vacancy. Finally, a correlation was found between the amount of methanol formed and the amount of  $SO_3$  adsorbed which supports our hypothesis that the active site for CO hydrogenation over  $ZrO_2$  is an oxygen anion vacancy.

#### ACKNOWLEDGMENTS

This work was supported by the Division of Chemical Sciences, Office of Basic Energy Sciences, U.S. Department of Energy, under Grant DE-FG05-86ER13604. The Fourier transform infrared spectrometer was funded by the Department of Defense Instrumentation Grant DAAG-29-83-0097. The XPS measurements were performed by J. Cook. We also thank T. Jin for helpful comments.

#### REFERENCES

- Pichler, H., and Ziesecke, K.-H., *Brennst. Chem.* **30**, 360 (1950).
- Pichler, H., and Ziesecke, K.-H., *Bur. Mines Bull.*, 448 (1950).
- Tseng, S. C., Jackson, N. J., and Ekerdt, J. G., *J. Catal.* **109**, 284 (1988).
- Maehashi, T., Maruya, K.-I., Domen, F., Aika, K.-I., and Onishi, T., *Chem. Lett. Chem. Soc. Japan*, 747 (1984).
- Abe, H., Maruya, K.-I., Domen, K., and Onishi, T., *Chem. Lett. Chem. Soc. Japan*, 1875 (1984).
- He, M.-Y., and Ekerdt, J. G., *J. Catal.* **90**, 17 (1984).
- Jackson, N. B., and Ekerdt, J. G., *J. Catal.* **101**, 90 (1986).
- Yamaguchi, T., Jin, T., and Tanabe, K., *J. Phys. Chem.* **90**, 3148 (1986).
- Jin, T., Yamaguchi, T., and Tanabe, K., *J. Phys. Chem.* **90**, 4794 (1986).
- Bensitel, M., Saur, O., Lavalley, J.-C., and Morrow, B. A., *Mater. Chem. Phys.* **19**, 147 (1988).
- McCullough, J. D., and Trueblood, K. N., *Acta Crystallogr.* **12**, 507 (1959).
- Evans, P. A., Stevens, R., and Binner, J. G. P., *Trans. J. Brit. Ceram. Soc.* **83**, 39 (1984).
- Scott, H. G., *J. Mater. Sci.* **10**, 1527 (1975).
- Garvie, R. C., *J. Phys. Chem.* **69**, 1238 (1965).
- Etsell, T. H., and Flengas, S. N., *Chem. Rev.* **70**, 339 (1970).
- Heyne, L., in "Mass Transport in Oxides," National Bureau of Standards Special Publication 296, p. 149, 1968.
- Kingerly, W. D., Pappis, J., Doty, M. E., and Hill, D. C., *J. Amer. Ceram. Soc.* **42**, 393 (1959).

18. Dexpert-Ghys, J., Faucher, M., and Caro, P., *J. Solid State Chem.* **84**, 179 (1984).
19. Catlow, C. R. A., Chadwick, A. V., Greaves, G. N., and Moroney, L. M., *J. Amer. Ceram. Soc.* **69**, 272 (1986).
20. Kilner, J. A., and Steele, B. C. H., in "Non-stoichiometric Oxides" (O. T. Sorensen, Ed.). Academic Press, New York, 1981.
21. Catlow, C. R. A., *Solid State Ionics* **12**, 67 (1984).
22. He, M.-Y., and Ekerdt, J. G., *J. Catal.* **87**, 238 (1984).
23. Ingel, R. P., and Lewis, D., III, *J. Amer. Ceram. Soc.* **69**, 325 (1986).
24. He, M.-Y., and Ekerdt, J. G., *J. Catal.* **87**, 381 (1984).
25. Silver, R. G., Jackson, N. B., and Ekerdt, J. G., in "Catalytic Activation of Carbon Dioxide" (W. M. Ayers, Ed.), ACS Symposium Series 363 1988.
26. Morrow, B. A., McFarlane, R. A., Lion, M., and Lavalley, J. C., *J. Catal.* **107**, 232 (1987).
27. Simpson, L. A., and Carter, R. E., *J. Amer. Ceram. Soc.* **49**, 139 (1966).
28. Nowick, A. S., Wang, D. Y., Park, D. S., and Griffith, J., in "Fast Ion Transport in Solids" (P. Vashishta, J. N. Mundy, and G. K. Shenoy, Eds.), p. 673. North-Holland, Amsterdam, 1979.
29. Gerhardt-Anderson, R., and Nowick, A. S., *Solid State Ionics* **5**, 547 (1981).
30. Srivastava, K. K., Patil, R. N., Choudhary, C. B., Gokhale, K. V. G. K., and Subbarao, E. C., *Trans. J. Brit. Ceram. Soc.* **73**, 85 (1974).
31. Mackrodt, K. W. C., and Woodrow, P. M., *J. Amer. Ceram. Soc.* **69**, 277 (1986).
32. Morinaga, M., Cohen, J. B., and Faber, J., Jr., *Acta Crystallogr.* **A35**, 789 (1979).
33. Morinaga, M., Cohen, J. B., and Faber, J., Jr., *Acta Crystallogr.* **A36**, 520 (1980).
34. Butler, C. V., Catlow, C. R. A., and Fender, B. E. F., *Radiat. Eff.* **73**, 273 (1983).
35. Figueras, F., Figlarz, M., Portefaix, J. L., Forisier, M., Gerand, B., and Guenot, J., *J. Catal.* **71**, 389 (1981).
36. Tatibouet, J. M., Phichitkul, Ch., and Germain, J. E., *J. Catal.* **99**, 231 (1986).
37. Germain, J. E., in "Adsorption and Catalysis on Oxide Surfaces" (M. Che and G. C. Bond, Eds.), p. 355. Elsevier, Amsterdam 1985.